FAILURE BEHAVIOR OF 3D-BRAIDED COMPOSITES MODELING BY A MULTI-SCALE VARIATIONAL APPROACH

D. Bigaud, P. Hamelin

Laboratoire Mécanique Matériaux L2M, Université Claude Bernard Lyon I
43 blvd du 11 novembre 1918, 69622 Villeurbanne Cedex, France

SUMMARY: The purpose of this paper is to present the failure behavior modeling of 3D-braided composites. Two main parameters are considered to be predominant on the failure behavior; the variations of the yarns orientation, which generates a complex field of stresses, and the scattering of internal values of strength partly due to damages induced in the yarn during the manufacturing and consolidation steps.
A preliminary work has been done to identify the internal geometry of the braided composites. Once achieved, we propose a sub-cell modeling solution based on a multi-scale analysis allowing to locate and quantify the material rate and mechanical influence of each constituent (fiber or resin) within the composite. The analysis of the braided composite mechanical behavior finally consists in studying that of an aggregate of multi-scale sub-cells with individual properties. Theoretical results obtained show a good agreement with experiments carried out on a Carbon / PA12 3D-braided composite.

KEYWORDS: failure of 3D composites, braided composites, homogenization, variational principles.

INTRODUCTION

The literature generally shows two main approaches to consider the failure behavior of composites. The first one considers a global response of the composite up to failure. Then, yield criteria (Hill, Tsaï-Wu…) are applied to describe the material macroscopic behavior. In this case, the criteria formalism does not systematically take into account the fracture mechanisms involved. The second approach is based on the observation of fracture phenomena. This observation proves that the composite failure generally consists in mixed effects of fiber rupture, matrix cracking and debonding at the fiber / matrix interface that can lead to delamination.
In the specific case of 3D-braided composites, the macroscopic failure follows from local fracture of yarns and no more from matrix cracking or delamination phenomena. The classical criteria become inaccurate and one needs to define an approach adapted to the local analysis of stress heterogeneity and to the description of the braiding yarns spatial evolution within the reinforcement.

INTERNAL GEOMETRY OF A 3D CARTESIAN BRAIDED COMPOSITE

Four-step Cartesian braiding technique

The braided preforms of the present study have been made by using the four-step Cartesian braiding technique and in collaboration with the Institut Textile de France. This technique was analyzed and adapted by many authors in the last ten years [1][2]. The step number indicates the number of sequences required for a machine cycle (Fig. 1). The first step consists in the shift of the yarns attached to the rows. The second step implies the shift of the columns. The third and fourth steps respectively present the inverse movements of the steps one and two.

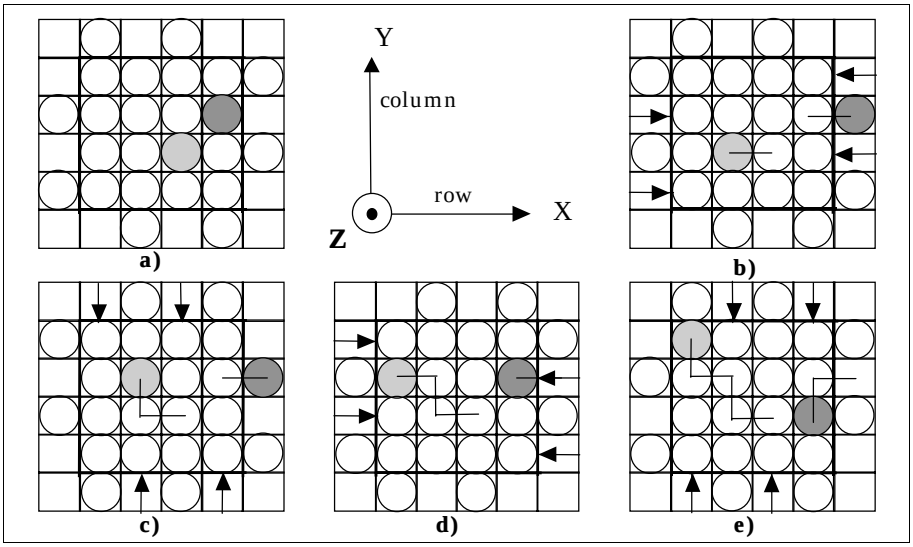

Fig. 1: The four-step Cartesian braiding technique.

The braided preform obtained is reinforced in its whole volume and may present a significant thickness and a complex section in which the braiding yarns are interlaced to such a degree that one cannot distinguish separated layers. Figs. 2a and 2b show the photographs of 3D Cartesian braided preform and composite.

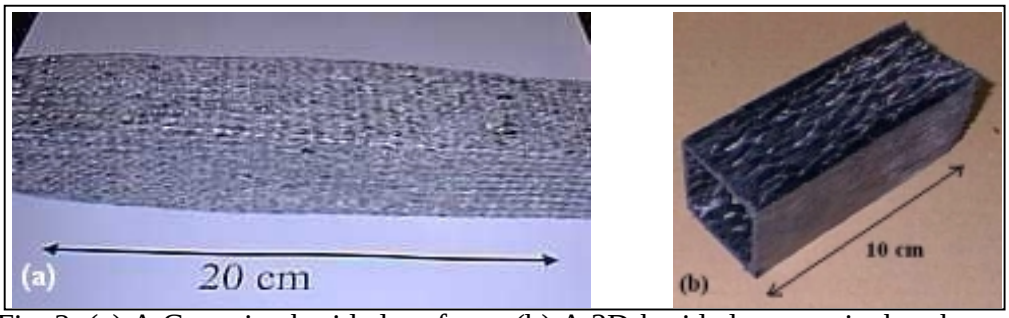

Fig. 2: (a) A Cartesian braided preform. (b) A 3D-braided composite box beam.

Internal geometry identification

This 3D-braided composite is a very heterogeneous structure. As a consequence, the stress and strain fields within it depend greatly on the constituents repartition, on their size and on their spatial arrangement. In other words, it depends on the textile internal geometry.
The only acquaintance of the braiding visible angle θ_v and the yarns diameter d – called braiding principal parameters (Fig. 3)- is not enough to describe the yarns path and, then, to identify the unit cell of a consolidated Cartesian braid. Thus, we have proceed to the sectioning of a rectangular braided composite (obtained according to the scheme described in

Fig. 1 with ten columns and three rows) and made micrographies at several successive plans parallel to (x,y). Next, each micrography is digitized and treated in order to restitute the yarns contour (Fig. 4). The study of the evolution of yarns (x,y) position for consecutive z-values allows the 3D reconstruction of an idealized braided unit cell (Fig. 5). The yarns path equations are derived from classical polynomial functions and the section equation can be chosen among elliptical, lenticular, rectangular or horse-track shape functions.

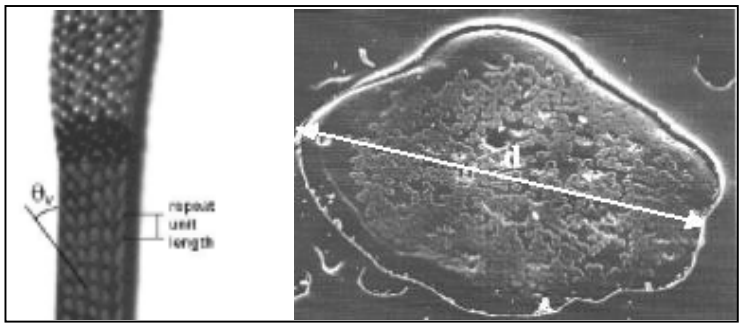

Fig. 3: The braiding principal parameters θ_v (visible braiding angle) and d (yarn diameter).

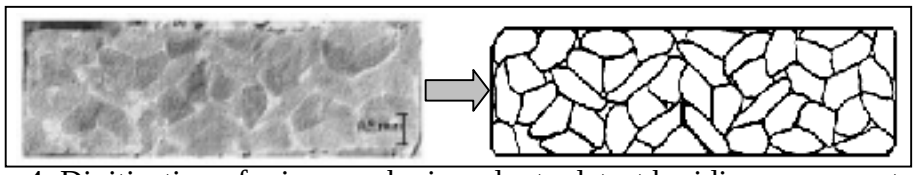
Fig. 4: Digitization of micrography in order to detect braiding yarns contour.

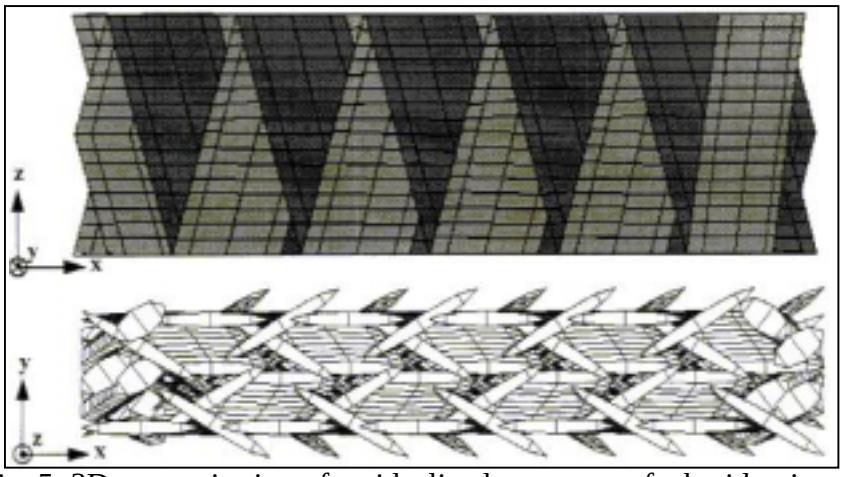

Fig. 5: 3D reconstitution of an idealized geometry of a braid unit cell.

MULTI-SCALE MODELING

Multi-scale meshing

Once the geometrical description achieved, we begin to study the mechanical modeling. A brief bibliography shows the interest to use a sub-cell analysis. It allows to determine the stress and strain internal states; essential condition to a study of the failure behavior. This sub-cell analysis is associated with a multi-scale analysis which aims at taking into account the various mechanisms implied at different material scales during the composite damage.
So as to illustrate with the simplest possible way the multi-scale meshing [3], we propose to study the case of a single yarn (Fig. 6a) extracted from the braid unit cell. To this unit cell, and, a fortiori to this yarn, we superimposed a meshing of regular intermediate elements (Fig. 6b). These elements have eight nodes that define as many mesoscopic elements (Fig. 6c). If

the entire node does not belong to the drawn volume of yarn then the associated meso-element is of resin type. On the contrary, the associated meso-element is of yarn type and possess the mechanical characteristics of a fiber / matrix mixture modeled by an assembly of four microscopic elements (Fig. 6d) and presenting the local spatial orientation derived by minimizing the distance between the meso-element center and the yarn path.
The main feature of this multi-scale meshing is to offer the opportunity to separate and to localize the resin, yarn and fiber zones and, then, to take into account the whole actual phenomena that are implied during the unit cell damage.

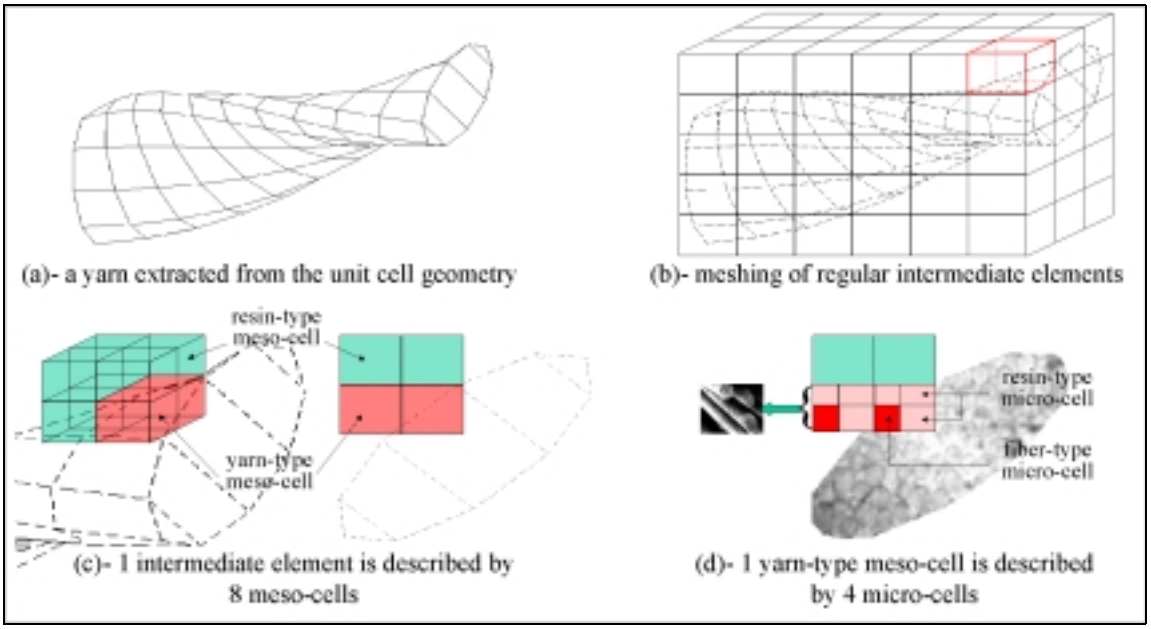

Fig. 6: The multi-scale meshing technique.

Use of this multi-scale meshing for the failure modeling of 3D-braided composites

For each scale, we have to define the mechanical characteristics of 2D or 3D elements as a function of sub-elements individual properties. A numerical procedure based on stationary functions derived from complementary and strain energy is developed.
The main idea of the method consists in making stationary both the complementary U_σ and the strain U_ε energy. This is done in order to define the lower and upper bounds of the effective stiffness and the internal strain and stress values of the unit cell ($\equiv N_x N_y N_z$ intermediate elements). In the case of the intermediate elements, we have $N_x=N_y=N_z=2$ (one intermediate element $\equiv$ eight meso-elements). In the case of the meso-elements, we have $N_x=N_y=2$ and $N_z=1$ (one meso-element $\equiv$ four micro-elements).
U_σ and U_ε are expressed as:

$$\begin{aligned} U_\sigma &= \frac{1}{2}\sum_{p=1}^{N_x N_y N_z} v_p \{\sigma\}_p^T [s]_p \{\sigma\}_p = \frac{1}{2}\{\Sigma\}^T [S]\{\Sigma\};\ \{\Sigma\}=\{\overline{\sigma}\}=\{\overline{\sigma}_1,\ldots,\overline{\sigma}_6\};\ \{\sigma\}_p=\{\sigma_{1,p},\ldots,\sigma_{6,p}\} \\ U_\varepsilon &= \frac{1}{2}\sum_{p=1}^{N_x N_y N_z} v_p \{\varepsilon\}_p^T [c]_p \{\varepsilon\}_p = \frac{1}{2}\{E\}^T [C]\{E\};\ \{E\}=\{\overline{\varepsilon}\}=\{\overline{\varepsilon}_1,\ldots,\overline{\varepsilon}_6\};\ \{\varepsilon\}_p=\{\varepsilon_{1,p},\ldots,\varepsilon_{6,p}\} \end{aligned} \quad (1)$$

Where v_p, $\{\sigma\}_p$, $\{\varepsilon\}_p$, $[s]_p$ and $[c]_p$ represent respectively the volume ratio, the stress and strain tensors, the compliance and stiffness matrix of the sub-cell p. $\{\Sigma\}$, $\{E\}$, $[S]$ and $[C]$ represent the average (or macroscopic) tensors of stress and strain and the average compliance and stiffness matrix.

By means of Lagrangian multipliers, one can take into account the conditions of continuity and averaging of stress (U_σ) and strain (U_ε) and write the new functionals U_σ^* and U_ε^*:

$$\begin{aligned} U_\sigma^* &= U_\sigma + \lambda_i f\left(\{\Sigma\},\{\sigma\}_p\right) \\ U_\varepsilon^* &= U_\varepsilon + \alpha_i g\left(\{E\},\{\varepsilon\}_p\right) \quad \lambda_i, \alpha_i : \text{Lagrangian multiplier} \end{aligned} \tag{2}$$

One can then write the conditions $\partial U_\sigma^* = 0$ and $\partial U_\varepsilon^* = 0$ as:

$$\begin{aligned} [K_\sigma]\begin{Bmatrix}\{\sigma\}_p \\ \{\lambda_i\}\end{Bmatrix} &= \begin{Bmatrix}\{0\}_p \\ \{\Sigma\}\end{Bmatrix} \\ [K_\varepsilon]\begin{Bmatrix}\{\varepsilon\}_p \\ \{\alpha_i\}\end{Bmatrix} &= \begin{Bmatrix}\{0\}_p \\ \{E\}\end{Bmatrix} \end{aligned} \tag{3}$$

Solving Eqn 3 for the sub-elements stress and strain allows to relate the sub and the total average vectors [4]:

$$\begin{aligned} \{\sigma\}_p &= \left[\ell^\sigma\right]^p \{\Sigma\} \\ \{\varepsilon\}_p &= \left[\ell^\varepsilon\right]^p \{E\} \end{aligned} \tag{4}$$

Then the upper and lower bounds of the $N_xN_yN_z$-cells assembly effective stiffness can be written as:

$$\left[\sum_{p=1}^{N_xN_yN_z} v_p [s]_p \left[\ell^\sigma\right]^p\right]^{-1} \le [C] \le \sum_{p=1}^{N_xN_yN_z} v_p [c]_p \left[\ell^\varepsilon\right]^p \tag{5}$$

By writing Eqn 4 as:

$$\begin{aligned} \{\sigma\}_p &= \left[\ell^\sigma\right]^p [C]\{E\} = [c]_p \left[\ell^\varepsilon\right]^p [C]^{-1}\{\Sigma\} \\ \{\varepsilon\}_p &= \left[\ell^\varepsilon\right]^p [C]^{-1}\{\Sigma\} = [s]_p \left[\ell^\sigma\right]^p [C]\{E\} \end{aligned} \tag{6}$$

and by using Eqn 5, one can estimate the bounds of the internal strain and stress according to imposed external strain and stress up to the micro-cells scale. The knowledge of yarns internal stresses and strains is directly exploitable to anticipate the composite failure behavior that is considered as a sequence of yarns local fractures.

FAILURE CRITERIA AT THE MESO-ELEMENTS SCALE

General aspects

In any 3D composite, the macroscopic failure generally results from local failures of yarns and not from phenomena linked to matrix cracking. It is essentially due to the reduction of the fiber / matrix interface and to the disappearance of matrix pockets. Cox [5] reports that the failure of 3D composites is restricted to phenomena combining axial tension and compression and yarn shear (kink band formation) failures, which the resin does not affect.
Then, instead of using a too microscopic approach, we choose to directly integrate the failure criteria (tensile and shear strength) at the meso-scale of the model (at the scale of the yarns) in order to avoid the errors done when changing from the filaments to the yarns scale. We also

take the choice to consider the scattering of local values of strength partly due to damages induced in the yarn during the manufacturing and the consolidation processes by studying a statistical distribution of those values.

Tensile tests on braiding yarns

Yarns made of Carbon fibers spun with PA12 thermoplastic matrix (fiber volume ratio: V_f=60%) are extracted from the braided preforms and consolidated at 220°C under a seven-bar pressure during one hour in order to simulate the consolidation cycle of the Cartesian braided composites. Next, glass / epoxy tabs are placed at the consolidated yarns ends.
The tensile strength is described by mean of a three-parameter Weibull law (Eqn 7) in order to take into account the influence of the yarn gauge length (this gauge length appears in the modeling in term of yarn length within a meso-element).

$$F_L(\sigma) = 1 - \exp\left[-\left(\frac{L}{L_0} \right)^{\alpha} \left(\frac{\sigma}{\sigma_{L_0}} \right)^{\beta} \right] \tag{7}$$

where $F_L(\sigma)$: the cumulative distribution function (CDF) of the yarn strength value,
σ: the stress applied to the yarn,
σ_{L_0} : the scale parameter,
β: the shape parameter,
α: a correlation factor which describes the gauge length effect ($0 \le \alpha \le 1$).

For each of the four different gauge lengths selected (35, 70, 105, 140 mm), we have carried out tensile tests on 23, 18, 18 and 15 samples. In fact, we have tested 32 yarns for each gauge length but we only keep results obtained from tests where the yarn has broken far from the tabs (Fig. 7). It appeared that the longer was the yarn the less the failure was localized at this level.
Then, we express the variation of the braiding yarn strength as a function of the CDF for a reference length L_i (F_{Li}) (Fig. 8).

$$\mathrm{Ln}\left[\mathrm{Ln}\left(1/\left(1 - F_{L_i}(\sigma)\right)\right)\right] = \beta_i \mathrm{Ln}(\sigma) - \left(\beta_i \mathrm{Ln}(\sigma_{L_i}) - \mathrm{Ln}(L_i)\right) \tag{8}$$

The shape and scale parameters β_i and σ_{Li}, the averages, standard deviations and variances for each length L_i are summed up in table 1.

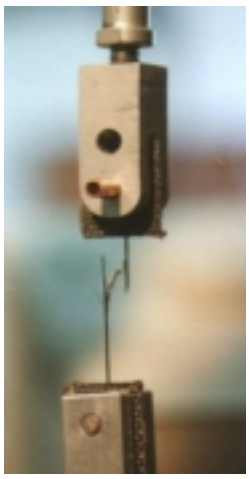

Fig. 7: Tensile test carried out on yarn elements.

Table 1: Weibull's law parameters β_i and σ_{Li} for each gauge length L_i – Averages,standard deviations and variances of the experimental values.

Gauge length L_i	*Scale parameter* σ_{Li}	*Shape parameter* β_i	*Averages* μ_i	*Standard deviations* ε_i	*Variance* S_i
L_0=35 mm	912	6.612	851	151	0.177
L_1=70 mm	890	6.548	830	148	0.178
L_2=105 mm	844	6.574	787	140	0.178
L_3=140 mm	770	7.330	722	116	0.161

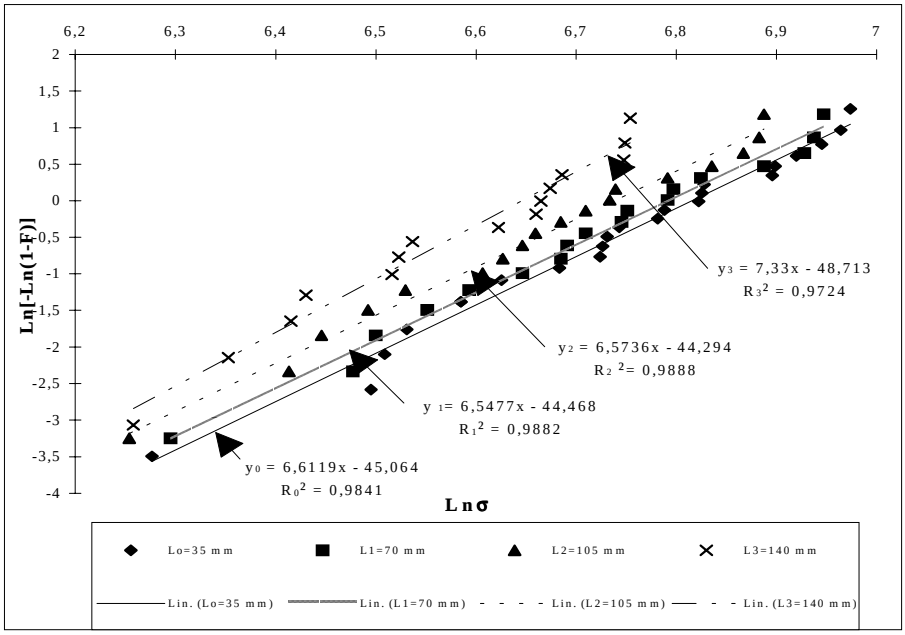

Fig. 8: Strength C.D.F. of the carbon / PA12 yarn for various gauge length.

In order to determine the third parameter of the Weibull's law α, we study the variations of $\sigma_{L_i}/\sigma_{L_o}$ as a function of L_i/L_0 (with L_0=35 mm) (see Fig. 9). The value of α is estimated to 0.61.

Finally, we can write the CDF of the carbon / PA12 yarn for any gauge length (Eqn 9).

$$F_L(\sigma) = 1 - \exp\left[-(L/35)^{0.61}(\sigma/912)^{6.612}\right] \tag{9}$$

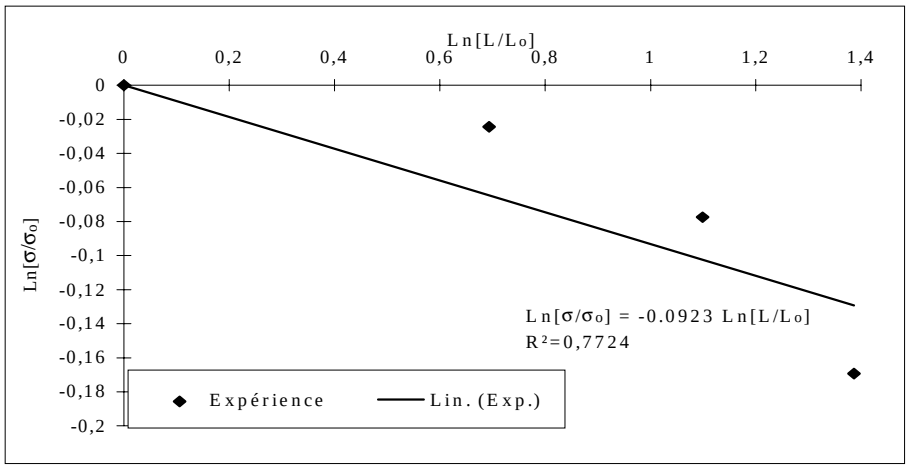

Fig. 9: Determination of the third parameter α - Variation of $Ln(\sigma_{Li}/\sigma_{Lo})$ as a function of $Ln(L_i/L_o)$.

Shear tests on braiding yarns

In the literature, we do not find any formalism dealing with the shear failure in terms of mechanical local phenomena. Intuitively, one may conceive that the shear strength decreases when the number of filaments within the yarn section increases, but in the same reinforcement, the same yarn, the number of filaments does not vary. For this reason, we choose to model the shear strength CDF by a two-parameter Weibull law.
The experimental device used to determine the shear strength is shown in Fig. 10a. The scheme of the test procedure is illustrated in Fig. 10b. Thirty samples of yarn with a length of 70 mm and an average area S_f of 0.8 mm² have been tested. For reason of loading symmetry, the shear stress is expressed as a function of the externally applied load P:

$$\tau_{xy} = \frac{P}{2S_f} \tag{10}$$

We find that the shear strength CDF matches the two-parameter Weibull's law below:

$$F(\tau) = 1 - \exp\left[-(\tau/96.8)^{12.683}\right] \tag{11}$$

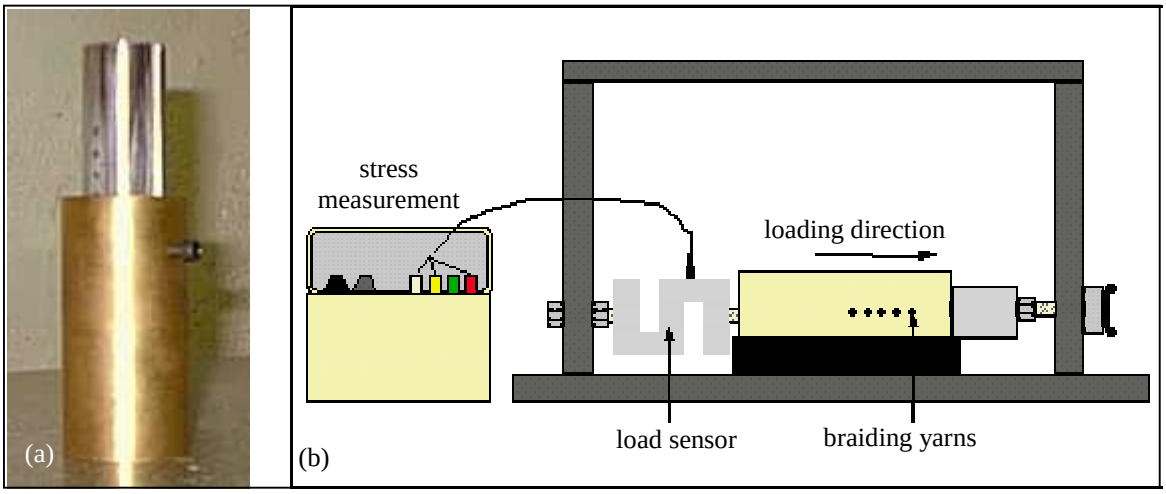

Fig. 10: Shear tests on yarns -a- shearing experimental device, -b- overview of the experimental setup.

Details on numerical procedure for progressive failure simulation

The procedure for failure simulation of the $N_xN_yN_z$-cells assembly according to an external mono-axial stress is detailed in Fig. 11.
First, the meso-elements strength under tensile and shear stress are randomly assigned to a Monte Carlo simulation. The bounds of the undamaged composite stiffness matrix are calculated in the next step. Next, by using Eqn 6, the local stresses within the meso-elements are determined according to an arbitrary external stress. They are compared to the critical stresses in order to investigate the macroscopic stress value that would yield to the failure of the first meso-element (yarn segment). The stiffness matrix of the meso-element is reduced by the selective RC method (rows and columns of the matrix $[c]_p$ set to zero according to the critical stress which was exceeded). The elastic analysis is carried on taking into account the drop of stress ($\Sigma_i \rightarrow \Sigma_{i'}$) and the change of unit cell stiffness matrix [C] (change of [S]).

EXPERIMENTAL VALIDATION OF THE THEORETICAL MODEL

Tensile tests are carried out on forty-three-yarn-braided-composites. The figure 12a shows a comparison between three experimental and the two progressive damage simulations (U_σ and U_ε).
In the case of the U_σ approach, the first simulated meso-element failure occurs before the one given by the U_ε approach (130 MPa according to U_σ and 180 MPa according to U_ε). The failure of the whole braided composite is then predicted before the one determined from the U_ε approach.
We remark that experimental curves are included between the bounds defined by our two variational approaches for strain values lower than 8000 µm/m. After that, discrepancies may be observed and we notice that the simulated stress and strain to failure values are lower than the experimental ones. This is partly due to the original formulation of the strength problem that is based on maximum stress criteria and to the fact that strain criteria are not taken into account. We can also explain this by the fact that debonding phenomena are not taken into account in our present model. However, we can conclude that our model provides a rather good trend as for the prediction of damage behavior of 3D Cartesian braided composite under mono-axial loading.

We conclude the study of 3D-braided composite failure by the influence of the braiding angle on the macroscopic tensile strength. We observe that the tensile strength value decreases from 805 to 87 MPa when θ_v varies from 10 to 50°. In term of internal stresses, we observe that the greater the visible braiding angle is, the more predominant become the local damages due to shear phenomena.

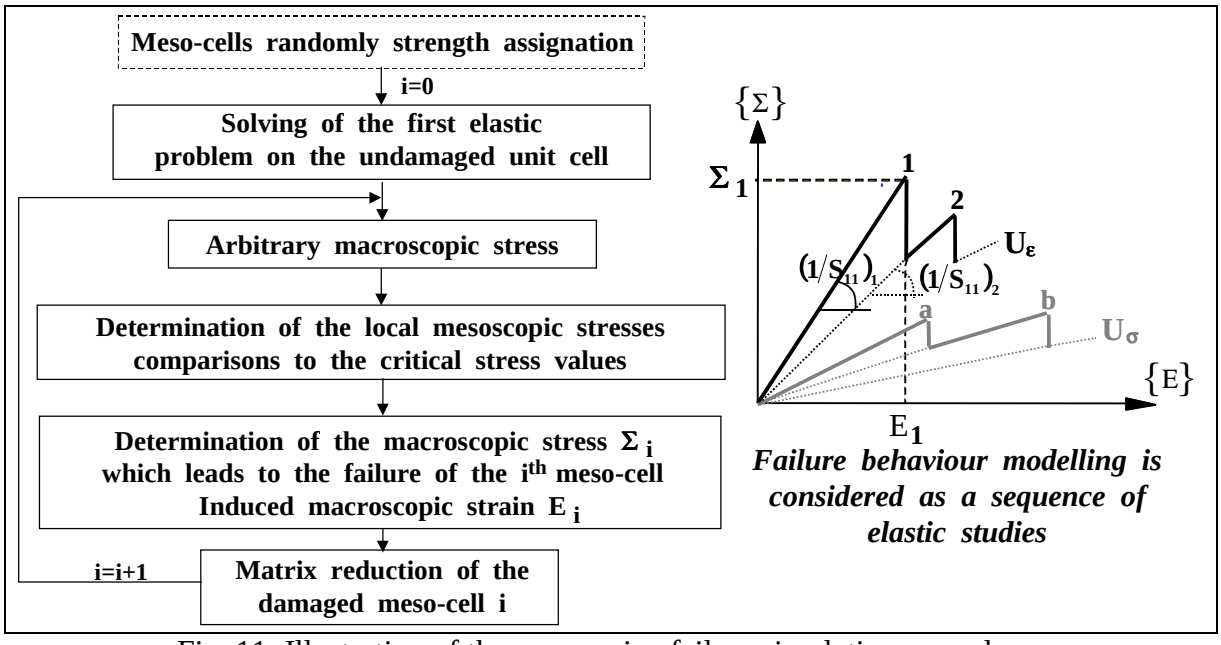

Fig. 11: Illustration of the progressive failure simulation procedure.

CONCLUSIONS

Homogenization techniques based on variational principles have been proposed in order to predict the damage behavior of 3D-braided composites. These techniques, which need the prior knowledge of the internal reinforcement geometry, have been adapted in order to study the composite macroscopic failure in term of tensile and shear local failures. First

comparisons between experimental and theoretical results have proved that the proposed approach can be used in order to give the trends of damage functions.

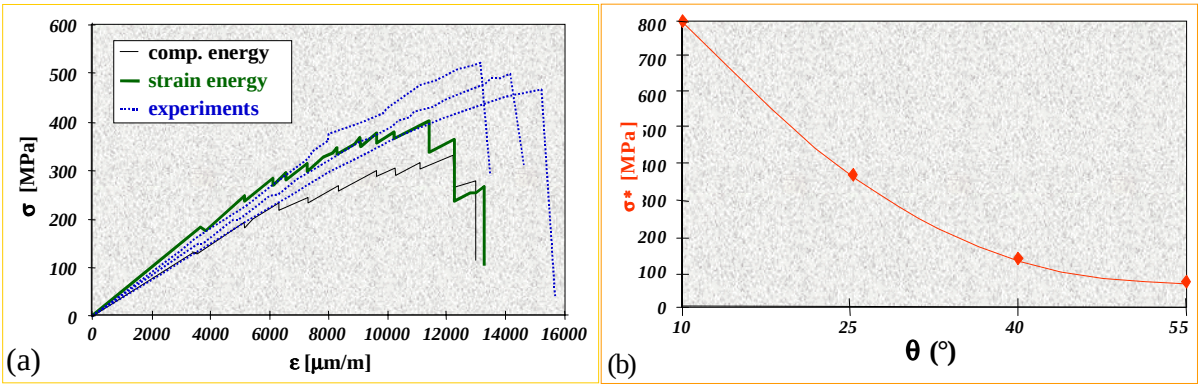

Fig. 12: (a) Comparisons between experimental and simulated damage functions in the case of a 3D-braided composite. (b) Influence of the braiding angle.

ACKNOWLEDGEMENTS

The present research is granted by the Institut Textile de France, the Rhône-Alpes region and the French Ministry of Research as part of a "Technologie Clef" program concerning the valorization of 3D textile technology for advanced composite materials.

REFERENCES

1. Pastore, C.M., "A processing science model for three dimensional braiding", Ph.D. thesis submitted to the University Drexel, USA, 1988.

2. Kostar, T.D. and Chou, T.W., "Process simulation and fabrication of advanced multi-step 3D braided preforms", *Journal of materials science*, Vol. 29, 1994, pp. 2159-2167.

3. Bonnel, P., "Modélisation géométrique et méthodes théorico-expérimentales d'identification des rigidités de composites à renforts textiles", Ph.D. thesis submitted to the University Claude Bernard Lyon 1, France, 1994.

4. Chen, D. and Cheng, S., "Analysis of composite materials: A micromechanical approach", *Journal of reinforced plastics and composites*, Vol. 12, 1993, pp. 1323-1338.

5. Cox, B.N. and Flanagan, G., "Handbook of analytical methods for textile composites", Ed. Rockwell Science Center, 1996.